Distributing Polarization Entangled Photon Pairs with High Rate over Long Distance through Standard Telecommunication Fiber

Lijiong Shen,[1] Chang Hoong Chow,[1] Justin Yu Xiang Peh,[1] Xi Jie Yeo,[1] Peng Kian Tan,[1] and Christian Kurtsiefer[1,2]

[1] *Centre for Quantum Technologies, National University of Singapore, 3 Science Drive 2, Singapore 117543*
[2] *Department of Physics, National University of Singapore, 2 Science Drive 3, Singapore 117551**

(Dated: June 6, 2022)

Distributing entanglement through standard telecommunication fiber is particularly important for quantum key distribution protocols with low vulnerability over metropolitan distances. However, entanglement distribution over long distance through optical fiber so far could only be accomplished with moderate photon pair rates. In this work, we present entanglement distribution over 50 km of standard telecommunication fiber with pair rate more than $10{,}000\,\mathrm{s}^{-1}$ using a bright non-degenerate photon pair source. Signal and idler wavelengths of this source are optimized for low dispersion in optical fiber and high efficiency for single-photon avalanche diode detectors, respectively. The resulting modest hardware requirement and high rate of detected entangled photon pairs could significantly enhance practical entanglement-based quantum key distribution in existing metropolitan fiber networks.

I. INTRODUCATION

Quantum entanglement is one of the most fascinating phenomena in quantum physics. It provides the foundation for applications like quantum teleportation, some variants of quantum key distribution (QKD) [1–4], or implementations of a quantum internet [5, 6].

In recent years, the rapid development of quantum technologies has driven QKD towards higher key generation rates [7] and longer distances — metropolitan area [8, 9], inter-city [10], and even inter-continental quantum communication has been demonstrated recently [11]. Currently, building secure quantum networks on top of these point-to-point quantum communication schemes is of increasing interest in research and commercial applications [12].

Most implementations of QKD are based on prepare-and-measure protocols due to its optical simplicity. In contrast, entanglement-based QKD can offer the advantage of not requiring a trusted active random number generator [13], and is immune to photon number splitting attacks, exposing fewer vulnerabilities in a practical implementation [14]. Moreover, entanglement is also the basis of device-independent quantum cryptography, a class of higher-security QKD schemes that does not rely on the premise that the involved devices can be trusted [15, 16]. Thus, it is highly desirable to distribute entanglement over long distance for future quantum secure networks.

While distributing entanglement over very long distance through free space [17] or even satellite links [18] is naturally appealing due to the low optical transmission loss in air, optical fibers can guide photons over the long distance without challenging alignments or environmental considerations. They also are the sole option when a line-of-sight is unavailable. Optical fibers are a particularly attractive transmission method in metropolitan areas, where ITU G.652D standard compliant fiber is likely already deployed as part of their existing telecommunication infrastructure [19].

Early work has demonstrated distribution of polarization-entangled photons through fiber over 1.45 km [20] for relatively short wavelengths. Polarization entanglement is much easier to prepare, measure, and couple to other physical systems compared to time-bin entanglement [21], which is a common encoding scheme at telecom wavelengths because it requires fewer expensive detectors. Time-bin entanglement is also less susceptible to polarization degradation due to polarization mode dispersion (PMD) in optical fibers, an effect that is severe for broadband photons found in many sources of polarization-entangled photons [22]. Improved technology continuously lowered the PMD of optical fibers, and permitted to manufacture low loss optical filters to reduce photon bandwidth. Consequently, polarization entanglement distribution over tens or even more than 100 km optical fiber has been demonstrated in recent years [23–26].

However, these demonstrations had to make optimizations that limit their practicality. For example, dispersion-shifted fibers (typically G.655 standard compliant fibers) have lower transmission losses and dispersion at 1550 nm compared to G.652D fibers [27], but are far less deployed in existing telecommunication networks. Alternatively, chromatic dispersion and PMD could be reduced by using narrow band pass filters together with conventional entangled pair sources, but this reduces the heralding efficiency of photon pairs even for ideal spectral filters with unity transmission in pass band [28], eventually leading to a lower entangled photon pair detection rate. Consequently, most reported work on long distance entanglement distribution was carried out with photon pair rates that are too low for most practical applications. Similarly, superconducting nanowire single-photon detectors (SNSPDs) are used in many demonstrations of long distance entanglement distribution due to their high efficiency, low dark counts, and low timing jitter [29].

* christian.kurtsiefer@gmail.com

However, SNSPDs need to be cooled below 4 K, which requires a significant overhead in power, size, and cost in comparison with typical single-photon avalanche photodiodes (APDs).

In this work, we present a highly non-degenerate entangled photon pair source based on type-0 spontaneous parametric down-conversion (SPDC) process to overcome these drawbacks in fiber-based entanglement distribution. One of the photons in pairs has a wavelength of 1310 nm and falls in the zero-dispersion window of G.652D standard compliant fiber, and a sub-nanometer bandwidth even without any spectral filtering. The other photon in the pairs has a wavelength around 586 nm where Si-APDs have nearly optimal detection efficiency. With such a source, we observe an average entanglement visibility of more than 97% locally. After transmitting the 1310 nm photons through 50 km of G.652D compliant fiber, we still observe a photon pair coincidence rate over 10,000 s^{-1} with a pair of APDs, with a raw polarization entanglement visibility of 92.5%. The corresponding estimated quantum key rate in a BBM-92 like protocol [4] with such a source would be 5,172 s^{-1}. This is a significant boost in rates for practical quantum key distribution in a metropolitan area.

II. EXPERIMENTAL SETUP

A sketch of the experimental setup is shown in Fig. 1. Time-correlated photon pairs are generated via SPDC in a periodically poled potassium titanyl phosphate crystal (PPKTP, $2 \times 1 \times 20\,mm^3$) that is pumped with light from a grating-stabilized diode laser at a wavelength of 405 nm. An α-BBO crystal splits the pump light into two paths of orthogonal polarizations (horizontal, H, and vertical, V) with a beam separation of 1 mm through birefringence. A half-wave plate (HWP) transforms the H polarized pump light part back to V. The type-0 SPDC process in both conversion paths generates photon pairs in a state $|VV\rangle$, which then are separated by wavelength using a dichroic mirror. The polarization of the separated signal and idler photons from one of the pump paths is transformed to horizontal by two HWPs designed for their respective wavelengths. With this, the crystal generates $|VV\rangle$ and $|HH\rangle$ photon pairs in the different pump paths of the same crystal, which are then spatially overlapped by two α-BBO crystal beam splitters, one in each collection path to take care of the different birefringent properties at signal and idler wavelengths. The entanglement of photons arises from the indistinguishability between the photon pairs generated in the two down-conversion paths [30, 31]. By adjusting the relative power and phase between the two pump paths, the maximally entangled state

$$|\Phi^-\rangle = \frac{1}{\sqrt{2}}(|HH\rangle - |VV\rangle)$$

can be prepared.

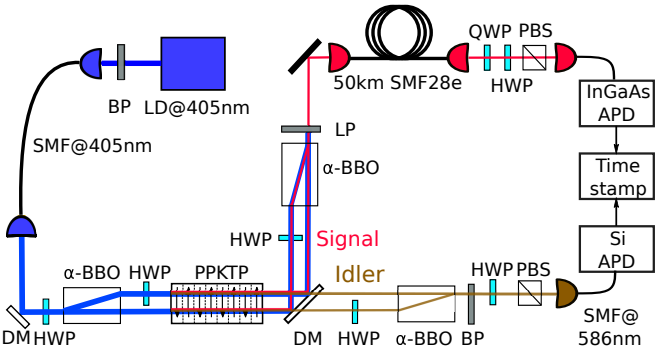

FIG. 1. Schematic of the non-degenerate entangled photon pair source. Pump light at 405 nm is split into two paths and is subject to type-0 SPDC inside the PPKTP crystal. The polarization state in the upper path is rotated by 90 degrees by a half-wave plate. Each pump path generates photon pairs with a non-degenerate wavelength at 1310 nm (signal), and 586 nm (idler). A dichroic mirror (DM) separates the non-degenerate photons from both pump paths. A pair of α-BBO crystals recombine the two signal and two idler paths separately to create an entangled state $|\Phi^-\rangle = \frac{1}{\sqrt{2}}(|HH\rangle - |VV\rangle)$. A motorized HWP and a PBS projects idler photons into different polarizations. Signal photons at 1310 nm are first coupled into a long SMF28e+ telecommunication fiber before projection into linear bases in a similar way as the idler photons.

Both a long pass (LP) filter with a cutoff wavelength at 1200 nm and a bandpass (BP) filter with a bandwidth of 20 nm centered at 586 nm effectively remove pump light from the individual collection path. A timestamp unit records the photon arrival time on both InGaAs-APD (timing jitter $\approx$ 250ps) and Si-APD (timing jitter $\approx$ 500ps) to look for coincidences. We choose a coincidence window of 1.25 ns to capture the majority of the photon pairs for all the measurements reported in this work.

The pair generation rate of the source is first characterized without the entanglement mechanism mediated by the beam displacers. At a pump power of 100 μW, a pair rate of more than 10,000 s^{-1} is observed with over 20% heralding efficiency; this value increases to 22% after correction for detector dark counts and after-pulses. It is worth noting that even with a relatively optimistic estimation of the detector efficiency (60% for the Si-APD, and 15% for the InGaAs-APD), the ideal heralding efficiency assuming a perfect fiber coupling while ignoring losses on multiple optical elements is predicted to be $\sqrt{(15\% \times 60\%)} = 30\%$ (see Appendix A). This implies a close to optimal collection efficiency. The single rate at the Si-APD exceeds 70,000 s^{-1} with a pump power of 100 μW. Assuming a Si-APD efficiency of 60%, we can safely infer that at a pump power of 1 mW, the source should generate more than 1 million photon pairs in a second; a direct measurement would have severely saturated the available detectors.

Figure 2(a) shows a spectrum of the signal photons recorded with a grating spectrometer, with only a sin-

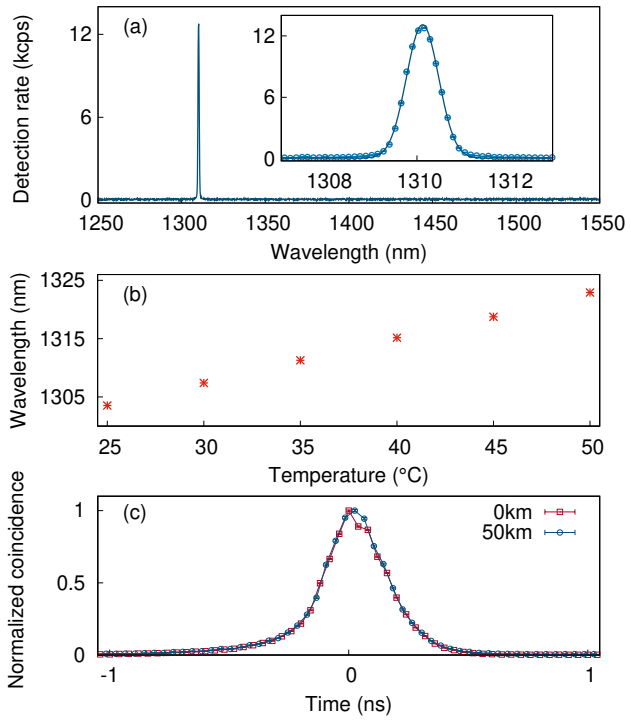

FIG. 2. (a) The spectrum of signal photons from the non-degenerate pair source at a temperature of 33.4 °C of the PPKTP crystal shows a single peak around 1310 nm with a nearly Gaussian profile (see fit to data in Inset). (b) Signal photon wavelength dependence on PPKTP temperature. (c) Time correlation of photon detection events from a pair of APDs, with the signal photon passing through 0 km and 50 km of SMF28e+ fiber, respectively. The temporal correlations for the 50 km transmission case are offset and normalized for visual comparison. Both histograms show a nearly indistinguishable distribution with a FWHM around 280 ps.

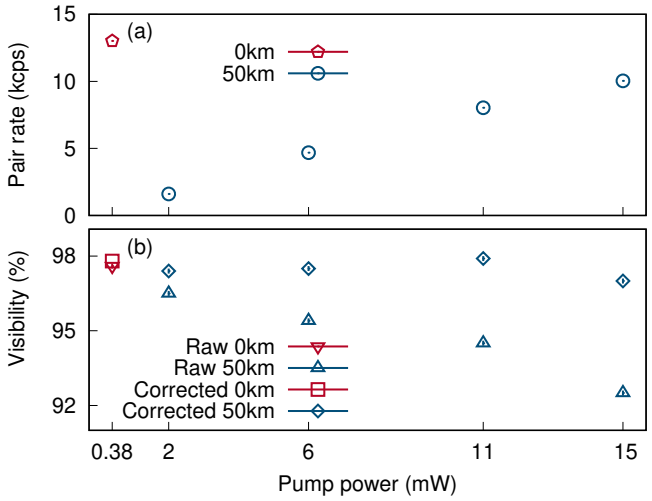

FIG. 3. (a) Average pair rates for different pump powers. The locally collected photon pair rate, averaged over H/V and D/A bases, is 13,012±14 s^{-1} at 380 μW pump power. Pair rates with the 50 km fiber in the signal arm are 1,606 ± 3 s^{-1}, 4,686±6 s^{-1}, 8,033±10 s^{-1}, and 10,033±16 s^{-1} at their corresponding pump powers. (b) Visibility of polarization correlations as a measure of entanglement quality for different pump powers. The raw visibility observed locally with 380 μW pump is 97.6±0.1%. After propagating through 50 km of SMF28e+ fiber, the raw visibility reduces to 96.5±0.1%, 95.4±0.1%, 94.5±0.1%, and 92.5±0.1% for a respective pump power of 2, 6, 11, and 15 mW. Background-corrected visibilities range from 97 % to 98 % for all the measurements.

gle peak in a range of 300 nm, with a center wavelength of 1310.12 nm and a Full Width at Half Maximum (FWHM) of 0.84 nm obtained from a fit to a Gaussian distribution. The spectrometer resolution is separately determined to be 0.47 nm (FWHM) with a distributed feedback laser at 1310 nm and a bandwidth of 3 MHz. Thus, the de-convoluted bandwidth of the source signal photons at 1310 nm is around 0.7 nm, corresponding to 120 GHz. Figure 2(b) shows the change of the center wavelength of signal photons with the temperature of the PPKTP crystal. The wavelength increases almost linearly with a slope of 0.8 nm/K over the zero-dispersion range (1304 nm-1324 nm) of the SMF28e+, G652D-compliant fiber.

To experimentally verify the zero-dispersion property of the fiber on signal photons, we carried out a coincidence measurement on photon pairs from the source with and without the 50 km fiber. For better timing resolution, the Si-APD was replaced with a device with smaller timing jitter (<40 ps) but lower detector efficiency (40%). The coincidence peak is shifted by around 247 μs for the measurement with the 50 km fiber. Both coincidence measurements are normalized to their maximum coincidence rate for easier visual comparison. Figure 2(c) clearly shows that the dispersion is unnoticeable even with the fast Si-APD.

III. ENTANGLEMENT DISTRIBUTION

The entanglement quality measurements were first carried out locally with the three α-BBO beam displacer inserted in the source, and polarization projections in signal and idler paths are implemented as shown in Fig. 1. To characterize entanglement, we extracted the visibility of polarization correlations in different bases, details are explained in Appendix B. The additional optics slightly reduces the source heralding efficiency from 22% to 18% for both pump paths. At 380 μW pump power, a raw visibility of 99.7±0.1% for the horizontal/vertical (H/V) basis, and 95.5±0.1% for the diagonal/anti-diagonal (D/A) basis is measured without 50 km delay fiber, resulting in an average raw visibility of 97.6±0.1% (97.8±0.1% after correcting for background coincidences, see Appendix C). The corresponding coincidence rate averaged over H/V and D/A bases is 13,012±14 s^{-1}.

Then, the 50 km SMF28e+ fiber (-17 dB loss) is in-

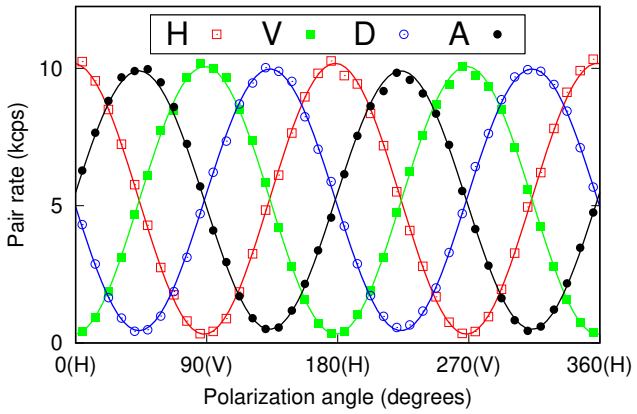

FIG. 4. Polarization correlations in both H/V and D/A bases measured at 15 mW pump power after transmission of the signal photons through 50 km SMF28e+ fiber. The coincidence rate is measured with polarization optics before signal and idler photon detection, as shown in Fig. 1. The polarization on the idler side is kept at one of the four linear settings (H, V, D, A) while the polarization on signal side is rotated over 360 degrees using the half wave plate.

serted between the source and the polarization analyzer on the signal branch. The observed coincidence rates and visibilities for different pump powers are shown in Fig. 3. As expected, the coincidence rate increases mostly linearly with pump power. We attribute the small nonlinearity at 15 mW pump power to an onset of saturation of the Si-APD (at a detection rate of $3.8 \times 10^6\,\mathrm{s}^{-1}$; specified maximum count rate $3 \times 10^7\,\mathrm{s}^{-1}$). The raw average visibility of the polarization correlation decreases with the pump power due to the quadratically increasing background coincidence (lower panel). However, after correcting the visibility for background coincidences, the visibility of polarization correlations and hence the quality of entanglement remains at an almost constant high level with no strong dependence on the pump power.

The raw visibility at 15 mW pump power is 94.0±0.1% in the H/V basis, and 91.0±0.2% in the D/A basis, corresponding to an average visibility of 92.5±0.1% (see Fig. 4). After correction for background coincidences, the average visibility at 15 mW pump power reaches 97.1±0.1%. The pair rate averaged over H/V and D/A bases is $10{,}033 \pm 16\,\mathrm{s}^{-1}$. Assuming that the measurement basis is chosen randomly and uniformly, that noise parameters are independent of measurement settings, and using a realistic bidirectional error correction efficiency value of 1.1 [32, 33], the estimated key distribution rate in a BBM-92 protocol would be $5{,}172\ \mathrm{s}^{-1}$.

IV. CONCLUSION

We present an entangled photon-pair source that is suitable for long distance quantum communication over the most deployed optical fiber compliant with the G.652D standard. The pair source generates signal photons at the zero-dispersion wavelength (1310 nm), while the corresponding idler photons have a wavelength of 586 nm, which is close to the optimal efficiency of typical Si-APDs. The source has a brightness of more than 10^6 pairs/s/mW. With the close to ideal mode matching that can be accomplished with it, more than 10,000 s^{-1} pairs are observed locally at 100 μW pump power using a pair of APDs. Entangled photon pairs can be generated by beam-displacement interferometer with minimal loss in brightness, and show a visibility of polarization correlations of over 97 %.

The low intrinsic bandwidth of 0.7 nm of signal photons in the conversion process strongly suppresses temporal dispersion of photons passing through 50 km SMF28e+, G652D-compliant optical fiber, and permits to use a narrow coincidence time window which helps to reject accidental coincidences that would deteriorate the observable entanglement quality. At the same time, an entangled photon pair rate of more than 10,000 s^{-1} with the same fiber can be detected with relatively simple avalanche photodetectors (APDs). With the usual error correction methods, this source/detection combination can be used to generate a secure bit rate of more than $5{,}000\,\mathrm{s}^{-1}$ in a BBM-92 protocol using simple polarization encoding [32, 33]. With the presented source, entanglement distribution can easily be extended to distances beyond 100 km at a rate of hundreds of pairs/second, without switching to more sophisticated superconducting single-photon detectors. To our knowledge, the entangled pair rate is at least an order of magnitude higher than other pair sources over the similar distance, despite the larger fiber attenuation per unit length in the O-band compared to the C-band [23–25]. Moreover, QKD applications using photons in the O-band have the advantage in that the quantum signal can co-propagate with light of classical internet traffic in C-band over the same fiber link [34]. We therefore believe that such a source can significantly improve entanglement distribution over metropolitan distances, permitting an integration of high-rate entanglement-based quantum key distribution into existing telecommunication network with realistic detection devices.

ACKNOWLEDGEMENTS

This work has been financially supported by the Quantum Engineering Programme through QEP-P1: Superconducting Nanowire and NRF2021-QEP2-04-P01: National Quantum-Safe Network, as well as the Ministry of Education and the National Research Foundation, Prime Minister's Office, Singapore.

APPENDIX A: HERALDING EFFICIENCY

Assuming a photon pair production rate P in the down conversion crystal, single photon detectors with efficiencies η_1 and η_2 will report single photon rates $S_{1(2)} = P\eta_{1(2)}$, where $\eta_{1,2}$ are total efficiencies, which include optical transmission, collection efficiencies through mode matching, and detection efficiencies of the single-photon detectors. A coincidence is registered when a photodetection event from each detector fall in a coincidence window τ_c. With negligible accidental coincidences, a coincidence rate $C = P\eta_1\eta_2$ can be observed.

The heralding efficiency η of the photon pair is defined as the pair to singles ratio [35] $C/\sqrt{S_1 S_2}$. Substituting coincidence and single rates with the above expressions leads to $\eta = \sqrt{\eta_1\eta_2}$. Assuming ideal mode matching without any transmission loss, the total efficiency $\eta_{1(2)}$ in each collection path is just the corresponding detector efficiency.

APPENDIX B: VISIBILITY MEASUREMENT

A combination of a HWP and a PBS (T_p:T_s > 1000:1) projects the polarization before coupling into the spatial mode selection fiber for the idler photon (586 nm). A similar free-space polarization measurement scheme is used for signal photons, where an additional quarter wave plate (QWP) is used to remove the ellipticity after fiber passage; in this path, polarization elements HWP and PBS are also placed behind the long fiber. On the idler side, four different polarizations (horizontal, H, vertical, V, diagonal, D, and anti-diagonal, A) are chosen by setting the HWP accordingly. On the signal side, the orientation of the linear polarization is changed in finer steps by rotating the HWP to obtain a visibility of the polarization correlations via $V = (C_{\max} - C_{\min})/(C_{\max} + C_{\min})$, where $C_{\max}$ and $C_{\min}$ are extracted from a sinusoidal fit to polarization correlations shown in Fig. 4.

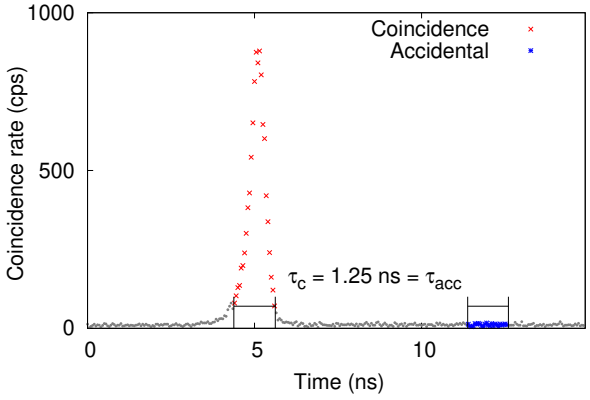

FIG. 5. Correlation of photon detection events from a pair of APDs for entanglement distribution, with the signal photon passing through 50 km of SMF28e+ fiber. The horizontal axis for the time difference is offset by about 247 μs. We consider detection events as coincidences when they fall into the time interval τ_c (width: 1.25 ns), and and measure the coicnidence rate in a time window $\tau_{\rm acc}$ of the same width, displaced by about 7 ns.

APPENDIX C: BACKGROUND CORRECTION

Apart from coincidences that can be attributed to photon pairs from the same SPDC process, we detect accidental coincidences from different pair generation processes, or from other detection processes. We estimate this accidental coincidence rate $C_{\rm acc}$ by recording the coincidence rate for time differences displaced by 7 ns from the main coincidence time window (see Fig. 5). Then, the coincidence rates are corrected by subtracting their respective accidental coincidence rate $C_{\rm acc}$ at each HWP angle. The corrected visibility is evaluated as $V = (C^{\rm corr}_{\max} - C^{\rm corr}_{\min})/(C^{\rm corr}_{\max} + C^{\rm corr}_{\min})$. The $C^{\rm corr}_{\max}$ and $C^{\rm corr}_{\min}$ are also extracted from a sinusoidal fit to the corrected polarization correlations.

[1] C. H. Bennett, G. Brassard, C. Crépeau, R. Jozsa, A. Peres, and W. K. Wootters, Phys. Rev. Lett. **70**, 1895 (1993).
[2] C. H. Bennett and G. Brassard, Proc. IEEE Int. Conf. Computers, Systems and Signal Processing , 175 (1984).
[3] A. K. Ekert, Phys. Rev. Lett. **67**, 661 (1991).
[4] C. H. Bennett, G. Brassard, and N. D. Mermin, Phys. Rev. Lett. **68**, 557 (1992).
[5] H. J. Kimble, Nature **453**, 1023 (2008).
[6] M. Pompili, S. L. Hermans, S. Baier, H. K. Beukers, P. C. Humphreys, R. N. Schouten, R. F. Vermeulen, M. J. Tiggelman, L. dos Santos Martins, B. Dirkse, *et al.*, Science **372**, 259 (2021).
[7] Q. Zhang, H. Takesue, T. Honjo, K. Wen, T. Hirohata, M. Suyama, Y. Takiguchi, H. Kamada, Y. Tokura, O. Tadanaga, Y. Nishida, M. Asobe, and Y. Yamamoto, New J. Phys **11**, 045010 (2009).
[8] Y.-L. Tang, H.-L. Yin, Q. Zhao, H. Liu, X.-X. Sun, M.-Q. Huang, W.-J. Zhang, S.-J. Chen, L. Zhang, L.-X. You, Z. Wang, Y. Liu, C.-Y. Lu, X. Jiang, X. Ma, Q. Zhang, T.-Y. Chen, and J.-W. Pan, Phys. Rev. X **6**, 011024 (2016).
[9] Y. Shi, S. Moe Thar, H. S. Poh, J. A. Grieve, C. Kurtsiefer, and A. Ling, Appl. Phys. Lett. **117**, 124002 (2020).
[10] A. Muller, H. Zbinden, and N. Gisin, Europhys. Lett. **33**, 335 (1996).
[11] S. K. Liao, W. Q. Cai, W. Y. Liu, L. Zhang, Y. Li, J. G. Ren, J. Yin, Q. Shen, Y. Cao, Z. P. Li, F. Z. Li, *et al.*, Nature **549**, 43 (2017).
[12] Y. A. Chen, Q. Zhang, T. Y. Chen, W. Q. Cai, S. K. Liao, J. Zhang, K. Chen, J. Yin, J. G. Ren, Z. Chen,

et al., Nature **589**, 214 (2021).
[13] I. Marcikic, A. Lamas-Linares, and C. Kurtsiefer, Appl. Phys. Lett. **89**, 101122 (2006).
[14] N. Lütkenhaus, Phys. Rev. A **61**, 052304 (2000).
[15] A. Acín, N. Brunner, N. Gisin, S. Massar, S. Pironio, and V. Scarani, Phys. Rev. Lett. **98**, 230501 (2007).
[16] V. Scarani, H. Bechmann-Pasquinucci, N. J. Cerf, M. Dušek, N. Lütkenhaus, and M. Peev, Rev. Mod. Phys. **81**, 1301 (2009).
[17] J. Yin, J. G. Ren, H. Lu, Y. Cao, H. L. Yong, Y. P. Wu, C. Liu, S. K. Liao, F. Zhou, Y. Jiang, *et al.*, Nature **488**, 185 (2012).
[18] J. Yin, Y. Cao, Y. H. Li, S. K. Liao, L. Zhang, J. G. Ren, W. Q. Cai, W. Y. Liu, B. Li, H. Dai, *et al.*, Science **356**, 1140 (2017).
[19] S. Wang, W. Chen, Z.-Q. Yin, H.-W. Li, D.-Y. He, Y.-H. Li, Z. Zhou, X.-T. Song, F.-Y. Li, D. Wang, *et al.*, Opt. Express **22**, 21739 (2014).
[20] A. Poppe, A. Fedrizzi, R. Ursin, H. R. Böhm, T. Lorünser, O. Maurhardt, M. Peev, M. Suda, C. Kurtsiefer, H. Weinfurter, T. Jennewein, and A. Zeilinger, Opt. Express **12**, 3865 (2004).
[21] I. Marcikic, H. de Riedmatten, W. Tittel, H. Zbinden, M. Legré, and N. Gisin, Phys. Rev. Lett. **93**, 180502 (2004).
[22] G. Ribordy, J. Brendel, J.-D. Gauthier, N. Gisin, and H. Zbinden, Phys. Rev. A **63**, 012309 (2000).
[23] H. Hübel, M. R. Vanner, T. Lederer, B. Blauensteiner, T. Lorünser, A. Poppe, and A. Zeilinger, Opt. Express **15**, 7853 (2007).
[24] A. Treiber, A. Poppe, M. Hentschel, D. Ferrini, T. Lorünser, E. Querasser, T. Matyus, H. Hübel, and A. Zeilinger, New J. Phys **11**, 045013 (2009).
[25] S. Wengerowsky, S. K. Joshi, F. Steinlechner, J. R. Zichi, S. M. Dobrovolskiy, R. van der Molen, J. W. Los, V. Zwiller, M. A. Versteegh, A. Mura, *et al.*, Proc. Natl. Acad. Sci. U.S.A. **116**, 6684 (2019).
[26] S. Wengerowsky, S. K. Joshi, F. Steinlechner, J. R. Zichi, B. Liu, T. Scheidl, S. M. Dobrovolskiy, R. v. d. Molen, J. W. Los, V. Zwiller, *et al.*, Npj Quantum Inf. **6**, 1 (2020).
[27] C. Inc., "Corning® LEAF® Optical Fiber Product Information," (2019).
[28] E. Meyer-Scott, N. Montaut, J. Tiedau, L. Sansoni, H. Herrmann, T. J. Bartley, and C. Silberhorn, Phys. Rev. A **95**, 061803(R) (2017).
[29] C. M. Natarajan, M. G. Tanner, and R. H. Hadfield, Supercond. Sci. Technol. **25**, 063001 (2012).
[30] M. Fiorentino and R. G. Beausoleil, Opt. Express **16**, 20149 (2008).
[31] A. Lohrmann, C. Perumangatt, A. Villar, and A. Ling, Appl. Phys. Lett. **116**, 021101 (2020).
[32] X. Ma, C.-H. F. Fung, and H.-K. Lo, Phys. Rev. A **76**, 012307 (2007).
[33] S. P. Neumann, T. Scheidl, M. Selimovic, M. Pivoluska, B. Liu, M. Bohmann, and R. Ursin, Phys. Rev. A **104**, 022406 (2021).
[34] J.-Q. Geng, G.-J. Fan-Yuan, S. Wang, Q.-F. Zhang, W. Chen, Z.-Q. Yin, D.-Y. He, G.-C. Guo, and Z.-F. Han, Opt. Lett. **46**, 6099 (2021).
[35] A. Joobeur, B. E. A. Saleh, and M. C. Teich, Phys. Rev. A **50**, 3349 (1994).